MOLECULAR PHYSICS, 2000, VOL. 98, NO. 4, 239–248

Monte Carlo simulation of a hard-sphere gas in the planar Fourier flow with a gravity field

E. E. TAHIRI[1], M. TIJ[2] and A. SANTOS[3]*

[1] Département de Mathématique, Université Moulay Ismaïl, Meknès, Morocco
[2] Département de Physique, Université Moulay Ismaïl, Meknès, Morocco
[3] Departamento de Física, Universidad de Extremadura, E-06071 Badajoz, Spain

(*Received 9 August 1999; revised version accepted 29 September 1999*)

By means of the Direct Simulation Monte Carlo (DSMC) method, the Boltzmann equation is numerically solved for a gas of hard spheres enclosed between two parallel plates kept at different temperatures and subject to the action of a gravity field normal to the plates. The profiles of pressure, density, temperature and heat flux are seen to be quite sensitive to the value of the gravity acceleration g. If the gravity field and the heat flux are parallel ($g > 0$), the magnitudes of both the temperature gradient and the heat flux are smaller than in the opposite case ($g < 0$). When considering the actual heat flux relative to the value predicted by the Fourier law, it is seen that, if $g > 0$, the ratio increases as the reduced local field strength increases, while the opposite happens if $g < 0$. The simulation results are compared with theoretical predictions for Maxwell molecules.

1. Introduction

The steady planar Fourier flow is one of the basic non-equilibrium states. It corresponds to a macroscopic system enclosed between two parallel infinite plates located at $z = 0$ and $z = L$ and kept at different temperatures T_- and T_+. After a certain transient period, the system reaches a steady state characterized by a temperature gradient $\partial T/\partial z$ along the direction z normal to the plates and a constant heat flux q_z. In the case of a fluid described by the Navier–Stokes equations, the heat flux is just proportional to the temperature gradient (Fourier law):

$$q_z^{\mathrm{NS}} = -\kappa(T(z))\frac{\partial T}{\partial z}, \tag{1}$$

where $\kappa(T)$ is the thermal conductivity coefficient, which, in general, depends on the local temperature T. In principle, the validity of the linear relation (1) is restricted to small gradients, i.e. to $\ell \gg \lambda$, where ℓ is the characteristic *hydrodynamic* length defined as $\ell = T|\partial T/\partial z|^{-1}$ and λ is a *microscopic* characteristic length (such as the mean free path in the case of a dilute gas). However, computer simulations of both dense fluids [1] and dilute gases [2, 3], as well as kinetic theory treatments [4–8] show that equation (1) is an excellent approximation even if $\ell \sim \lambda$. In the special case of dilute gases, Asmolov *et al.* [4] found an exact solution of the Boltzmann equation for Maxwell molecules [9] in which equation (1) is verified for *arbitrary* values of the thermal gradient. The same result is obtained from an exact solution [5] of the Bhatnagar–Gross–Krook (BGK) kinetic model [10] for any interaction potential.

The effect of gravity on the heat conduction of *dilute* gases is usually neglected. This is because the characteristic distance associated with gravity (i.e. the scale height $h = v_0^2/g$, where v_0 is the thermal velocity and g is the gravity acceleration) is much larger than ℓ and λ under usual laboratory conditions. Thus, the Fourier law (1) still holds if $h \gg \ell \sim \lambda$. On the other hand, an interesting question, from a physical point of view, is whether or not the heat conduction is influenced by a gravity field $\mathbf{g}$ along the z direction when the conditions of rarefaction and/or the strength of the field are such that the ratio λ/h is not negligibly small. In the case of Earth's atmosphere, for instance, h varies only within a range of 5–10 km up to an altitude of 100 km [11, 12]. On the other hand, λ increases from 10^{-5} cm at the surface to tens of kilometres at an altitude of 500 km. Consequently, $\lambda/h \sim 10^{-11}$ at the surface but rapidly increases with the altitude, being $\lambda/h \sim 1$ at the base of the exosphere [11].

* Author for correspondence. e-mail: andres@unex.es

In the study of the gravity effect on the heat conduction the main quantity of interest is the *reduced thermal conductivity* coefficient $\kappa^*(\varepsilon, g^*)$, where

$$\kappa^* \equiv \frac{q_z}{q_z^{\mathrm{NS}}}, \tag{2}$$

$$\varepsilon \equiv \frac{\lambda}{\ell} = \lambda \left| \frac{\partial \ln T}{\partial z} \right|, \tag{3}$$

$$g^* \equiv \frac{\lambda}{h} = \frac{\lambda g}{2k_{\mathrm{B}}T/m}. \tag{4}$$

The quantity ε is a dimensionless measure of the thermal gradient over the scale of the mean free path, while g^* is a measure of the strength of the gravity field over the same scale. In equation (4) we have identified the thermal velocity as $v_0 = (2k_{\mathrm{B}}T/m)^{1/2}$, where k_{B} is the Boltzmann constant and m is the mass of a particle. As a convenient definition of the mean free path we take

$$\lambda = \frac{2m\kappa v_0}{5k_{\mathrm{B}}p}, \tag{5}$$

where $p = nk_{\mathrm{B}}T$ is the hydrostatic pressure, n being the number density. The above definition of λ is based on the result for the thermal conductivity coefficient κ in the BGK model [13, 14]. It must be pointed out that all the quantities in (2)–(4) are *local*, i.e. they depend on z. For instance, κ^* is the ratio between the actual value of the heat flux (which is in fact uniform in the steady state) and the local value obtained from (1) with the actual local values of the temperature and its gradient. If the system is large enough ($L \to \infty$) and we restrict ourselves to the *bulk domain* (i.e. far from the boundaries), it is expected that all the space dependence of κ^* occurs through ε and g^* only.

The problem of elucidating the effect of $g^* \neq 0$ on the effective thermal conductivity κ^* has been recently addressed by us from a theoretical point of view [15–18]. In [15] the Boltzmann equation for Maxwell molecules was solved by a perturbation expansion through order g^2. The result is

$$\kappa^*(\varepsilon, g^*) = \kappa^*(\varepsilon, 0) + \tfrac{46}{5}\varepsilon g^* + \left(\tfrac{24}{5} + 503.7\varepsilon^2\right)g^{*2} + \mathcal{O}(g^{*3}), \tag{6}$$

where $\kappa^*(\varepsilon, 0) = 1$. Henceforth we take the convention that $g > 0$ when the field $\mathbf{g}$ is parallel to the heat flux vector $\mathbf{q}$ and $g < 0$ when $\mathbf{g}$ is antiparallel to $\mathbf{q}$. In the first case, according to equation (6), the heat transport is enhanced with respect to the Navier–Stokes prediction ($\kappa^* > 1$), while it is inhibited if $g < 0$. Of course, in the limit of a negligible field ($g^* \to 0$), the validity of the Fourier law for arbitrary ε [4] is recovered ($\kappa^* \to 1$). A similar analysis has been carried out in the context of the BGK model of the Boltzmann equation, also for Maxwell molecules [16]. This allowed us to perform the expansion through sixth order in the field, the behaviour of the numerical coefficients indicating that the series expansion is only *asymptotic*. The result to second order is

$$\kappa^*(\varepsilon, g^*) = \kappa^*(\varepsilon, 0) + \tfrac{58}{5}\varepsilon g^* + \left(\tfrac{32}{5} + \tfrac{47\,968}{25}\varepsilon^2\right)g^{*2} + \mathcal{O}(g^{*3}). \tag{7}$$

The asymptotic analysis of [16] agrees well with a finite-difference numerical solution of the BGK equation [17]. Comparison between equations (6) and (7) shows that the BGK model tends to overestimate the influence of the gravity field. A much more complex gravity effect appears in the planar Couette flow [18], where normal and shear stresses are present in addition to heat transport.

Thus far, all the previous studies about the influence of gravity on the heat conduction have been restricted to *Maxwell molecules*. In addition, most of them have been based on theoretical asymptotic analyses of the Boltzmann or BGK equations, the investigation of [17] being the only exception. The main merit of the Maxwell interaction is that it usually makes the analytic treatment of the Boltzmann equation more manageable, but otherwise it is a rather unrealistic potential. Structural, thermodynamic and transport properties of real fluids are much better captured by the hard-sphere model [19]. The aim of this paper is to investigate the gravity effect on the planar Fourier flow in the case of a dilute gas of *hard spheres* by solving numerically the Boltzmann equation by means of the DSMC method [20]. As will be seen, the simulation results agree qualitatively with the theoretical analyses. The physical problem is stated in section 2, where special attention is paid to the choice of the boundary conditions. The simulation method is described in section 3. Section 4 presents the results. Finally, the conclusions are summarized in section 5.

2. Planar Fourier flow in the presence of a gravity field

Let us consider a dilute gas of hard spheres enclosed between two parallel plates located at $z = 0$ and $z = L$. Both plates are maintained at temperatures T_- and T_+, respectively. Without loss of generality, we will assume that $T_+ > T_-$. In addition, a constant gravity field $\mathbf{g} = -g\hat{\mathbf{z}}$ is applied. Figure 1 presents a schematic illustration of the system geometry. Under these conditions, the Boltzmann equation reads [13, 14]

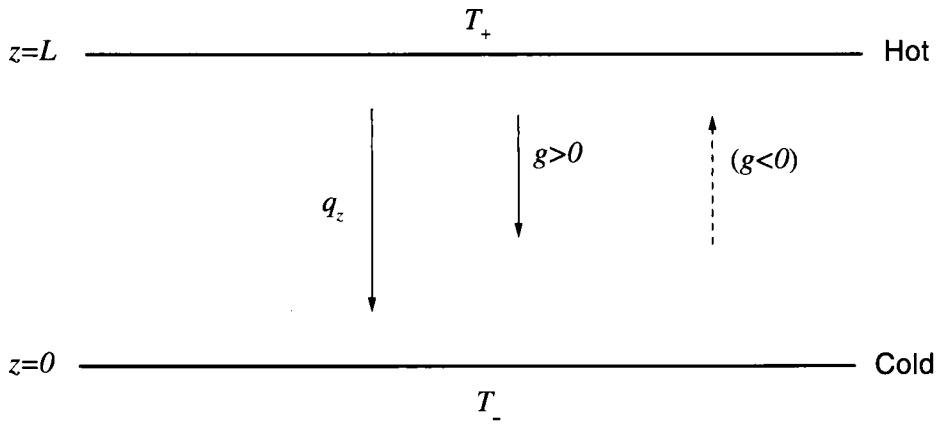

Figure 1. Schematic illustration of the system geometry.

$$\left(\frac{\partial}{\partial t}+v_z\frac{\partial}{\partial z}-g\frac{\partial}{\partial v_z}\right)f(z,\mathbf{v},t)=\sigma^2\int d\mathbf{v}_1\int d\hat{\boldsymbol{\sigma}}\Theta(\mathbf{g}\cdot\boldsymbol{\sigma})(\mathbf{g}\cdot\hat{\boldsymbol{\sigma}})\times[f(z,\mathbf{v}',t)f(z,\mathbf{v}_1',t)-f(z,\mathbf{v},t)f(z,\mathbf{v}_1,t)]. \quad (8)$$

Here, $f(z,\mathbf{v},t)$ is the one-particle velocity distribution function, σ is the diameter of a sphere, Θ is the Heaviside step function, $\mathbf{g}=\mathbf{v}-\mathbf{v}_1$ is the relative velocity, $\hat{\boldsymbol{\sigma}}$ is a unit vector in the direction of the line joining the centres of the two colliding particles, and $\mathbf{v}'=\mathbf{v}-(\mathbf{g}\cdot\hat{\boldsymbol{\sigma}})\hat{\boldsymbol{\sigma}}$ and $\mathbf{v}_1'=\mathbf{v}_1+(\mathbf{g}\cdot\hat{\boldsymbol{\sigma}})\hat{\boldsymbol{\sigma}}$ are post-collisional velocities. In equation (8) we have already assumed that, due to the geometry of the problem, the only relevant space coordinate is z. The hydrodynamic fields and the associated fluxes can be expressed as moments of the distribution function:

$$n(z,t)=\int d\mathbf{v}f(z,\mathbf{v},t), \quad (9)$$

$$\mathbf{P}(z,t)=m\int d\mathbf{v}\,\mathbf{v}\mathbf{v}f(z,\mathbf{v},t), \quad p=nk_BT=\tfrac{1}{3}\operatorname{Tr}\mathbf{P}, \quad (10)$$

$$\mathbf{q}(z,t)=\frac{m}{2}\int d\mathbf{v}\,v^2\mathbf{v}f(z,\mathbf{v},t). \quad (11)$$

In the expressions of the pressure tensor, equation (10), and of the heat flux, equation (11), we have assumed the absence of a flow velocity field. Multiplying equation (8) by (v_z,v^2) and integrating over velocity space, one gets the following *steady state* balance equations

$$\frac{\partial}{\partial z}P_{zz}+mng=0, \quad (12)$$

$$\frac{\partial}{\partial z}q_z=0. \quad (13)$$

In order to solve the Boltzmann equation (8) one needs to complement it with initial and boundary conditions. Since we will focus on the steady state, the particular choice of initial condition is not relevant here. As for the boundary conditions, they can be expressed in terms of the kernels $K_\pm(\mathbf{v},\mathbf{v}')$ defined as follows. When a particle with velocity $\mathbf{v}'$ hits the wall at $z=L$, the probability of being reemitted with a velocity $\mathbf{v}$ within the range $d\mathbf{v}$ is $K_+(\mathbf{v},\mathbf{v}')d\mathbf{v}$; the kernel $K_-(\mathbf{v},\mathbf{v}')$ represents the same but at $z=0$. The boundary conditions are then [21]

$$\Theta(\pm v_z)|v_z|f(z=\{0,L\},\mathbf{v},t)=\Theta(\pm v_z)\int d\mathbf{v}'\,|v_z'|K_\mp(\mathbf{v},\mathbf{v}')\times\Theta(\mp v_z')\times f(z=\{0,L\},\mathbf{v}',t). \quad (14)$$

In this paper we consider boundary conditions of complete accommodation with the walls, so that $K_\pm(\mathbf{v},\mathbf{v}')=K_\pm(\mathbf{v})$ does not depend on the incoming velocity $\mathbf{v}'$ and can be written as

$$K_\pm(\mathbf{v})=A_\pm^{-1}\Theta(\mp v_z)|v_z|\phi_\pm(\mathbf{v}),$$
$$A_\pm=\int d\mathbf{v}\,\Theta(\mp v_z)|v_z|\phi_\pm(\mathbf{v}), \quad (15)$$

where $\phi_\mp(\mathbf{v})$ represents the probability distribution of a fictitious gas in contact with the system at $z=\{0,L\}$. Equation (15) can then be interpreted as meaning that when a particle hits a wall, it is absorbed and then replaced by a particle leaving the fictitious bath. Of course, any choice of $\phi_\pm(\mathbf{v})$ must be consistent with the imposed wall temperatures, i.e.

$$k_B T_\pm = \tfrac{1}{3} m \int d\mathbf{v}\, v^2 \phi_\pm(\mathbf{v}). \tag{16}$$

The simplest and most common choice is that of a Maxwell–Boltzmann distribution:

$$\phi_\pm(\mathbf{v}) = \left(\frac{m}{2\pi k_B T_\pm}\right)^{3/2} \exp\left(-\frac{mv^2}{2k_B T_\pm}\right). \tag{17}$$

These boundary conditions have been frequently used in molecular dynamics simulations [1, 2] as well as in kinetic theory analyses [7, 8, 14, 17]. Under these conditions, the system is understood to be enclosed between two independent baths *at equilibrium* at temperatures T_+ and T_-, respectively. While the conditions (17) are adequate for analysing boundary effects [14, 22], they are not very efficient when one's interest lies with the transport properties in the bulk. In order to inhibit the influence of boundary effects, it is more convenient to imagine that the two fictitious baths are in *non-equilibrium* states resembling the state of the actual gas near the walls. More specifically, we can assume that the fictitious gases are described by the BGK equation, whose exact solution for the steady planar Fourier flow (in the absence of gravity) is known [6]. In which case,

$$\phi_\pm(\mathbf{v}) = \left(\frac{m}{2\pi k_B T_\pm}\right)^{3/2} \exp\left(-\frac{m(v_x^2 + v_y^2)}{2k_B T_\pm}\right)$$

$$\times \frac{(2k_B T_\pm/m)^{1/2}}{\varepsilon_\pm |v_z|} \int_0^\infty d\tau\, \Theta((1-\tau)\,\mathrm{sgn}\, v_z)\tau^{-3/2}$$

$$\times \exp\left[-(2k_B T_\pm/m)^{1/2} \frac{1-\tau}{\varepsilon_\pm v_z} - \frac{mv_z^2}{2k_B T_\pm \tau}\right], \tag{18}$$

where we have additionally assumed statistical independence among the three velocity components. In equation (18) $\varepsilon_\mp$ is the local reduced thermal gradient at $z = \{0, L\}$. If we formally take the limit $\varepsilon_\pm \to 0$, equation (18) reduces to equation (17) [6]. On the other hand, if $T_- \neq T_+$, then $\varepsilon_\pm \neq 0$. The exact solution of the BGK model [5, 6] has the properties $\partial T^{3/2}/\partial z = \text{const}$ (for hard spheres) and $p = \text{const}$; from them, it is easy to obtain

$$\varepsilon_\pm = \frac{15}{8(2\pi)^{1/2}} \frac{T_+^{1/2} - T_-^{1/2}}{\sigma^2 L \bar{n}} T_\pm^{-1/2}, \tag{19}$$

where

$$\bar{n} = \frac{1}{L} \int_0^L dz\, n(z) \tag{20}$$

is the average density. This second class of boundary conditions were first proposed in [3], where they proved to be much more efficient than the conditions (17) for the heat conduction problem. Following the same terminology as in [3], we will refer to the 'equilibrium' conditions (17) as conditions of Type I and to the 'non-equilibrium' conditions (18) as conditions of Type II.

3. Simulation method

In order to solve numerically the Boltzmann equation (8) with both types of boundary conditions, we have used the so-called DSMC method [20, 23]. Comparison with known exact solutions of the Boltzmann equation under strong non-equilibrium conditions [24] proves the reliability and efficiency of the DSMC method to solve the Boltzmann equation. In this method, the velocity distribution function is represented by the velocities $\{\mathbf{v}_i\}$ and positions $\{z_i\}$ of a sufficiently large number of particles N. Given the geometry of our problem, the physical system is split into layers of width Δz, sufficiently smaller than the mean free path. The velocities and coordinates are updated from time t to time $t + \Delta t$, where the time-step Δt is much smaller than the mean free time, by applying a convection step followed by a collision step. In the *convection step*, the particles are moved ballistically, i.e. $v_{iz} \to v_{iz} - g\Delta t$ and $z_i \to z_i + v_{iz}\Delta t - \frac{1}{2} g(\Delta t)^2$. In addition, those particles crossing the boundaries re-enter with velocities sampled from the corresponding probability distribution $K_\pm(\mathbf{v})$. The *collision step* proceeds as follows [20, 23]. For each layer α, a pair of potential collision partners, i and j, and a unit vector $\hat{\boldsymbol{\sigma}}_{ij}$ are chosen at random with equiprobability. The collision between particles i and j is then accepted with a probability equal to $\Theta(\mathbf{g}_{ij} \cdot \hat{\boldsymbol{\sigma}}_{ij})\omega_{ij}/\omega_{\max}$, where $\mathbf{g}_{ij} \equiv \mathbf{v}_i - \mathbf{v}_j$ is the relative velocity, $\omega_{ij} \equiv (\mathbf{g}_{ij} \cdot \hat{\boldsymbol{\sigma}}_{ij}) 4\pi\sigma^2 n_\alpha$ is the collision rate of the pair (i, j), n_α being the number density in layer α, and $\omega_{\max}$ is an upper bound estimate of the collision rate in the layer. If the collision is accepted, post-collisional velocities $\mathbf{v}'_{i,j} = \mathbf{v}_{i,j} \mp (\mathbf{g}_{ij} \cdot \hat{\boldsymbol{\sigma}}_i)\hat{\boldsymbol{\sigma}}_i$ are assigned to both particles. After the collision is processed or if the pair is rejected, the routine moves again to the choice of a new pair until the required number of candidate pairs $\frac{1}{2} N_\alpha \omega_{\max} \Delta t$ in the layer, where N_α is the total number of particles in layer α, has been processed.

In the course of the simulations, the following 'coarse-grained' local quantities are computed. The number density in layer α is

$$n_\alpha = \bar{n} \frac{N_\alpha}{(N/L)\Delta z} = \frac{\bar{n} L}{N \Delta z} \sum_{i=1}^{N} \Theta_\alpha(z_i), \tag{21}$$

where $\Theta_\alpha(z)$ is the characteristic function of layer α, i.e. $\Theta_\alpha(z) = 1$ if z belongs to layer α and is zero otherwise.

Similarly, the temperature, the pressure tensor and the heat flux of layer α are

$$k_B T_\alpha = \frac{p_\alpha}{n_\alpha} = \frac{m}{3N_\alpha}\sum_{i=1}^{N}\Theta_\alpha(z_i)v_i^2, \tag{22}$$

$$\mathbf{P}_\alpha = \frac{L}{N\Delta z}m\sum_{i=1}^{N}\Theta_\alpha(z_i)\mathbf{v}_i\mathbf{v}_i, \tag{23}$$

$$\mathbf{q}_\alpha = \frac{L}{N\Delta z}\frac{m}{2}\sum_{i=1}^{N}\Theta_\alpha(z_i)v_i^2\mathbf{v}_i. \tag{24}$$

According to equation (13), $\mathbf{q}$ is a constant in the steady state. Thus, we have also evaluated the *average* heat flux as

$$\bar{\mathbf{q}} = \frac{\Delta z}{L}\sum_\alpha \mathbf{q}_\alpha = \frac{1}{N}\frac{m}{2}\sum_{i=1}^{N}v_i^2\mathbf{v}_i. \tag{25}$$

The standard definition of mean free path in the case of hard spheres is [13]

$$\lambda' = \frac{1}{2^{1/2}n\pi\sigma^2}. \tag{26}$$

This quantity is not exactly the same as the mean free path defined by equation (5), which is based on the BGK model. The thermal conductivity of a dilute system of hard spheres is (in the first approximation) [13]

$$\kappa = \frac{75(\pi m k_B T)^{1/2}k_B}{64m\pi\sigma^2}, \tag{27}$$

so that $\lambda = (15\pi^{1/2}/16)\lambda'$. In the following, we take units such that $\bar{\lambda}' \equiv (2^{1/2}\bar{n}\pi\sigma^2)^{-1} = 1$ (length unit), $m = 1$ (mass unit), $(2k_BT_+/m)^{1/2} = 1$ (speed unit), $T_+ = 1$ (temperature unit) and $\bar{n} = 1$ (density level). The units of these and other related quantities are given in table 1. The table also gives the values of those units taking as a reference example a gas with $\sigma = 3$ Å, $m = 3\times10^{-26}$ kg, $T_+ = 10^3$ K and $\bar{n} = 4\times10^{15}$ m^{-3}, which are typical of the atmospheric conditions at an altitude of 220 km [12].

Table 1. Units used in this paper for the relevant quantities. The third column gives the 'real' values of those units taking $\sigma = 3$ Å, $m = 3\times10^{-26}$ kg, $T_+ = 10^3$ K and $\bar{n} = 4\times10^{15}$ m^{-3} as a reference example.

Quantity	Unit	Reference value
Temperature (T)	T_+	10^3 K
Mass (m)	m	3×10^{-26} kg
Length (z, L)	$\bar{\lambda}'$	625 m
Speed (v)	$(2k_BT_+/m)^{1/2}$	959 m s^{-1}
Time (t)	$\bar{\lambda}'(2k_BT_+/m)^{-1/2}$	0.652s
Acceleration (g)	$\bar{\lambda}'^{-1}(2k_BT_+/m)$	1.47×10^3 m s^{-2}
Number density (n)	$\bar{n}$	4×10^{15} m^{-3}
Pressure (p, P_{zz})	$\bar{n}(2k_BT_+)$	1.10×10^{-4} N m^{-2}
Heat flux (q_z)	$\bar{n}(2k_BT_+)^{3/2}m^{-1/2}$	0.106 J m^{-2} s^{-1}

Each physical situation is then characterized by the values of L, T_- and g only. In terms of quantities expressed in the above units, the reduced local parameters ε and g^*, defined by equations (3) and (4), are given as

$$\varepsilon = \frac{5\pi^{1/2}}{16pT^{1/2}}\left|\frac{\partial T^{3/2}}{\partial z}\right|, \tag{28}$$

$$g^* = \frac{15\pi^{1/2}}{32}\frac{g}{p}. \tag{29}$$

According to the Fourier law, equation (1), the heat flux is

$$q_z^{NS} = -\frac{25\pi^{1/2}}{64}\frac{\partial T^{3/2}}{\partial z}, \tag{30}$$

where we have taken into account that $\kappa \propto T^{1/2}$ for a hard-sphere gas and have used the identity $T^{1/2}\mathrm{d}T = \frac{2}{3}\mathrm{d}T^{3/2}$. Equation (30) implies that in the steady state described by the Fourier law one would have $\partial T^{3/2}/\partial z = \text{const}$. While this is not in general true, the slope of $T^{3/2}$ is expected to change more smoothly than that of T. This is why in equation (28) ε is written in terms of the former rather than in terms of the latter.

In the simulations we have taken $N = 5000$ particles, a layer width $\Delta z = 0.1$ and a time-step $\Delta t = 0.004$. We have started from initial conditions of the form

$$f(z,\mathbf{v},0) = n(z,0)\left(\frac{m}{2\pi k_B T(z,0)}\right)^{3/2}\exp\left[-\frac{mv^2}{2k_BT(z,0)}\right], \tag{31}$$

where $n(z,0) \propto 1/T(z,0)$ and $T(z,0) = T_-(1 + cz/L)^{2/3}$, with $c \equiv (T_+/T_-)^{3/2} - 1$. After a time period $t = 200$ the system has already relaxed to the steady state [3]. We follow the evolution of the system until $t = 2000$ and average the relevant quantities over 5000 snapshots equally spaced between $t = 200$ and $t = 2000$.

4. Results

By using the method outlined in the previous section, we have analysed 51 different states. In all of them, the separation between the plates has been taken as $L = 10$. Two different temperature ratios have been considered ($T_- = 0.01$ and $T_- = 0.05$) and boundary conditions of Types I and II have been applied. For each one of these four combinations, 12 or 13 different values of g have been taken, typically in the range $-0.024 < g < 0.014$. We illustrate in figures 2–5 the profiles found in the

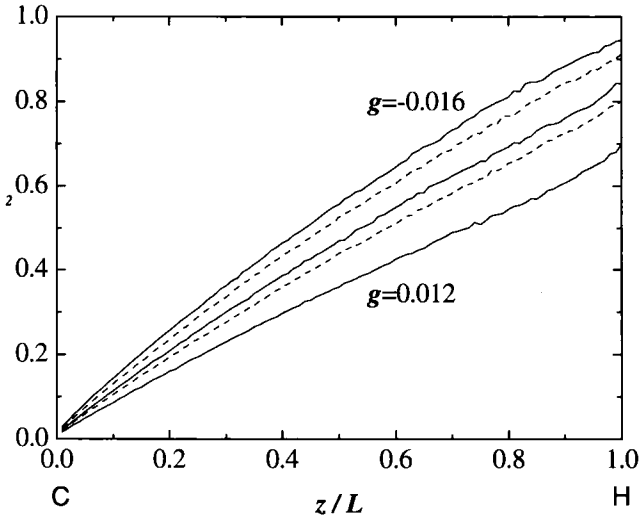

Figure 2. Profile of $T^{3/2}$ in the case $T_- = 0.05$ with boundary conditions of Type II. The values of g are, from top to bottom, $g = -0.016$, -0.008, 0, 0.008 and 0.012. The labels C and H denote the locations of the cold and hot walls, respectively.

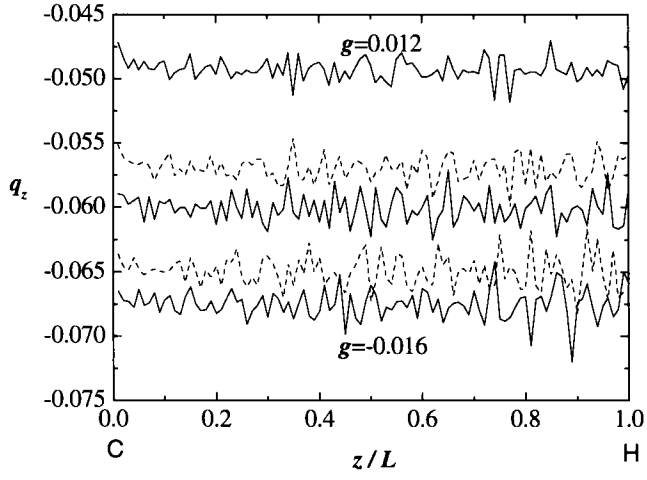

Figure 3. Profile of q_z in the case $T_- = 0.05$ with boundary conditions of Type II. The values of g are, from bottom to top, $g = -0.016$, -0.008, 0, 0.008 and 0.012. The labels C and H denote the locations of the cold and hot walls, respectively.

simulations by choosing the case $T_- = 0.05$ with boundary conditions of Type II as a reference example. The corresponding temperature profiles are shown in figure 2 for $g = -0.016$, -0.008, 0, 0.008 and 0.012. We observe that the temperature gradient is larger for $g < 0$ (i.e. when the gravity field is antiparallel to the heat flux) than for $g > 0$ (gravity field parallel to the heat flux). This implies that the magnitude of the heat flux is expected to be larger in the former case than in the latter. This is confirmed by figure 3, where the profile

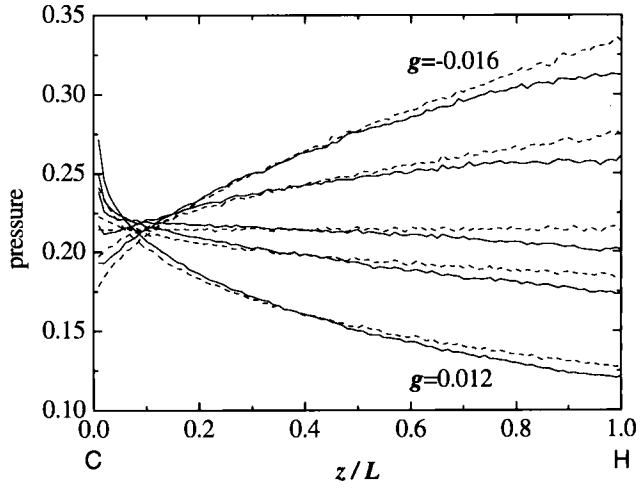

Figure 4. Profiles of p (—) and P_{zz} (- - -) in the case $T_- = 0.05$ with boundary conditions of Type II. The values of g are, from top to bottom at the right end, $g = -0.016$, -0.008, 0, 0.008 and 0.012. The labels C and H denote the locations of the cold and hot walls, respectively.

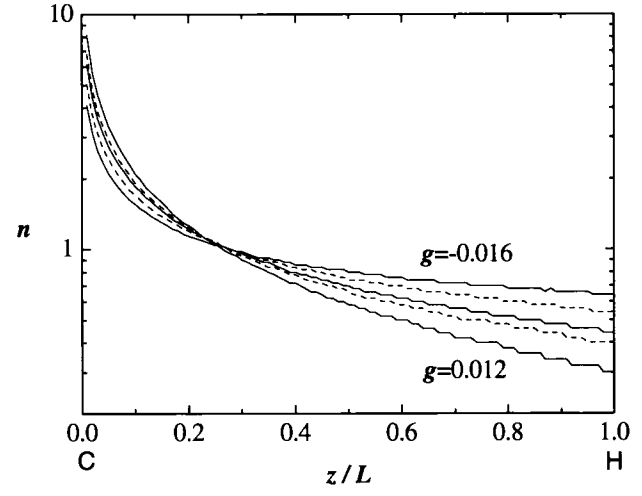

Figure 5. Profile of n in the case $T_- = 0.05$ with boundary conditions of Type II. The values of g are, from top to bottom at the right end, $g = -0.016$, -0.008, 0, 0.008 and 0.012. Note that the vertical axis is in logarithmic scale. The labels C and H denote the locations of the cold and hot walls, respectively.

of q_z is plotted for the same situations as in figure 2. Figure 3 also shows that, except for statistical fluctuations, the results are consistent with $q_z = \text{const}$. This is a consistency test that a steady state has been reached in the simulations (cf. equation (13)). The fact that the heat fluxes are constant and yet the profiles of $T^{3/2}$ are nonlinear can be traced back to local deviations from the Fourier law.

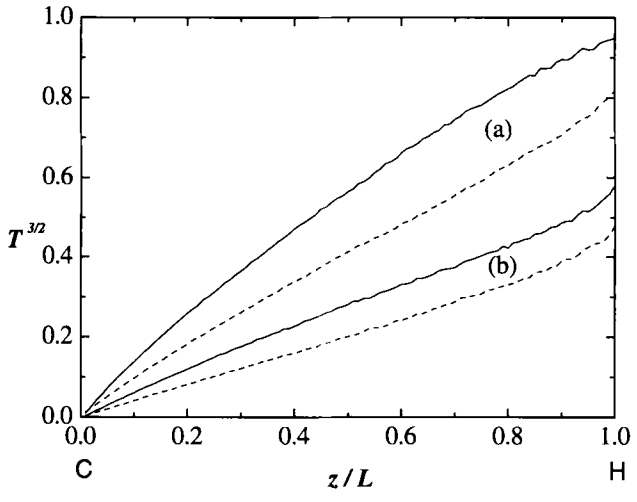

Figure 6. Profile of $T^{3/2}$ in the case $T_- = 0.01$ with boundary conditions of Types I (- - -) and II (—). The values of g are (*a*) $g = -0.016$ and (*b*) $g = 0.012$. The labels C and H denote the locations of the cold and hot walls, respectively.

The profiles of p and P_{zz} are shown in figure 4. At $g = 0$ the simulation results are consistent with a constant P_{zz}. On the other hand, in agreement with equation (12), P_{zz} is an increasing (decreasing) function of z when $g < 0$ ($g > 0$). The hydrostatic pressure p is slightly larger than P_{zz} for z/L smaller than about 0.3–0.4, while it is slightly smaller than P_{zz} for larger distances from the cold wall. It is worthwhile noting that the local density $n = 2p/T$ is much smaller in the hotter layers than in the colder ones, as seen in figure 5. Nevertheless, this disparity in the population of particles is widely influenced by the sign of g. Thus, for $g = -0.016$ the densities near the cold and hot walls are $n \simeq 4$ and $n \simeq 0.6$, respectively, while these values are $n \simeq 8$ and $n \simeq 0.3$ for $g = 0.012$. The large densities near the cold wall are responsible for the abrupt change of pressure in that region, in agreement with the balance equation (12).

In the cases $T_- = 0.05$ (with boundary conditions of Type I) and $T_- = 0.01$ (with boundary conditions of Types I and II) we have obtained results similar to those displayed in figures 2–5. The most interesting difference is that, as expected, the boundary effects are much less important when applying boundary conditions of Type II than those of Type I. This is illustrated in figure 6, where it can be seen that, given a value of L, T_- and g, the jump temperature at the walls is much smaller in the case for boundary conditions of Type II. This extends to $g \neq 0$ the observation made in [3] for $g = 0$.

As stated in section 1, we are mainly interested in investigating the influence of the gravity strength on the heat flux *relative* to the value predicted by the Navier–Stokes approximation with the actual thermal gradient. This ratio is the reduced thermal conductivity κ^*, equation (2). In the limit in which boundary effects are negligible ($L \to \infty$), it is expected that κ^* depends on position only through a functional dependence on the local parameters ε and g^*, defined by equations (3) and (4) or, equivalently, by equations (28) and (29) in our units. In order to minimize as much as possible the unavoidable boundary effects associated with a finite L, we will focus on the region around a point z_0 sufficiently far from both boundaries. By measuring the pressure, temperature and thermal gradient at $z = z_0$ (the heat flux is measured as the average value $\bar{q}_z$), we can compute the associated values of κ^*, g^* and $\varepsilon = \varepsilon_0$. The question arises as to how to choose the value of z_0. Here we have applied the following criterion. First, the value of z_0 for $g = 0$ is such that the expected number of collisions a particle experiences when going from $z = 0$ to $z = z_0$ or from $z = L$ to $z = z_0$ is 5, i.e. $\mathcal{N}(z_0) = 5$, where

$$\mathcal{N}(z) = \int_0^z \frac{dz'}{\lambda'(z')}. \tag{32}$$

Notice that, since $\lambda' = 1/n$ in our units, $\mathcal{N}(L) = L = 10$. In this way we have obtained $\varepsilon_0 = 0.33$ ($T_- = 0.05$, Type I), $\varepsilon_0 = 0.36$ ($T_- = 0.05$, Type II), $\varepsilon_0 = 0.44$ ($T_- = 0.01$, Type I) and $\varepsilon_0 = 0.48$ ($T_- = 0.05$, Type II), all of them with $g = 0$. If we followed the same method when choosing z_0 when $g \neq 0$, then we would obtain a different value of ε_0 each time and that would hinder the analysis of the *direct* influence of the gravity field on the coefficient κ^*. Therefore, for the second part of the criterion, we fix the above values of ε_0 for each of the four combinations of T_- and type of boundary conditions and then determine z_0 to accommodate the corresponding ε_0. The values of z_0, $\mathcal{N}(z_0)$, g^* and κ^* obtained in this way are given in tables 2–5. As we can see, the point z_0 is always closer to the cold wall than to the hot wall. However, when the separation is measured in terms of the number of collisions rather than as an actual distance, it turns out that the point z_0 is 'closer' to the hot wall, i.e. $\mathcal{N}(z_0) > 5$, if $g > 0$, while the opposite happens if $g < 0$.

In the absence of gravity ($g = 0$), we observe that κ^* is smaller than 1. This is in part due to a residual influence of boundary effects [3], as indicated by the fact that κ^* is closer to 1 with boundary conditions of Type II than with those of Type I. From the exact solution of the Boltzmann equation for an *unbounded* system of Maxwell molecules [4], it follows that $\kappa^* = 1$ for $g^* = 0$ and arbitrary ε. However, it is possible that $\kappa^*(\varepsilon, 0)$ is slightly smaller than 1 in the case of hard spheres, even if any boundary effect is removed. Thus, in order

Table 2. Values of z_0, $\mathcal{N}(z_0)$, g^*, κ^* and $\Delta\kappa^*$ for different values of g in the case $T_- = 0.05$ with boundary conditions of Type I. The values of z_0 are such that the reduced thermal gradient is $\varepsilon_0 = 0.33$.

g	z_0/L	$\mathcal{N}(z_0)$	g^*	κ^*	$\Delta\kappa^*$
−0.024	2.55	3.3	−0.095	0.903	−0.040
−0.020	2.55	3.5	−0.079	0.905	−0.038
−0.016	2.60	3.8	−0.063	0.906	−0.037
−0.012	2.60	4.1	−0.048	0.917	−0.026
−0.010	2.60	4.3	−0.040	0.921	−0.022
−0.008	2.55	4.3	−0.032	0.927	−0.016
−0.006	2.60	4.5	−0.025	0.934	−0.009
−0.004	2.50	4.5	−0.017	0.939	−0.004
0.000	2.70	5.0	0.000	0.943	0.000
0.003	2.80	5.3	0.013	0.951	0.008
0.006	2.85	5.6	0.028	0.969	0.026
0.008	2.90	5.8	0.039	0.978	0.035
0.010	3.20	6.3	0.052	0.986	0.043

Table 3. Values of z_0, $\mathcal{N}(z_0)$, g^*, κ^* and $\Delta\kappa^*$ for different values of g in the case $T_- = 0.05$ with boundary conditions of Type II. The values of z_0 are such that the reduced thermal gradient is $\varepsilon_0 = 0.36$.

g	z_0/L	$\mathcal{N}(z_0)$	g^*	κ^*	$\Delta\kappa^*$
−0.020	2.45	3.9	−0.068	0.908	−0.055
−0.016	2.45	4.1	−0.055	0.921	−0.042
−0.012	2.45	4.3	−0.042	0.934	−0.029
−0.010	2.40	4.4	−0.035	0.940	−0.023
−0.006	2.50	4.7	−0.022	0.949	−0.014
−0.003	2.50	4.9	−0.011	0.955	−0.008
0.000	2.50	5.0	0.000	0.963	0.000
0.004	2.60	5.5	0.016	0.983	0.020
0.008	2.60	5.5	0.032	0.988	0.025
0.010	2.90	6.2	0.046	1.016	0.053
0.012	3.00	6.4	0.058	1.036	0.073
0.014	3.55	7.0	0.077	1.064	0.101

Table 4. Values of z_0, $\mathcal{N}(z_0)$, g^*, κ^* and $\Delta\kappa^*$ for different values of g in the case $T_- = 0.01$ with boundary conditions of Type I. The values of z_0 are such that the reduced thermal gradient is $\varepsilon_0 = 0.44$.

g	z_0/L	$\mathcal{N}(z_0)$	g^*	κ^*	$\Delta\kappa^*$
−0.024	2.00	3.1	−0.108	0.833	−0.066
−0.020	2.00	3.4	−0.091	0.838	−0.061
−0.016	2.00	3.6	−0.073	0.838	−0.061
−0.014	2.00	3.8	−0.065	0.849	−0.050
−0.012	1.95	3.9	−0.056	0.861	−0.038
−0.008	2.00	4.3	−0.038	0.871	−0.028
−0.004	2.00	4.6	−0.020	0.880	−0.019
0.000	2.05	5.0	0.000	0.899	0.000
0.004	2.15	5.5	0.022	0.917	0.018
0.006	2.40	6.0	0.036	0.921	0.022
0.008	2.70	6.5	0.052	0.930	0.031
0.010	3.00	7.0	0.074	0.964	0.065
0.011	3.50	7.5	0.092	0.994	0.095

Table 5. Values of z_0, $\mathcal{N}(z_0)$, g^*, κ^* and $\Delta\kappa^*$ for different values of g in the case $T_- = 0.01$ with boundary conditions of Type II. The values of z_0 are such that the reduced thermal gradient is $\varepsilon_0 = 0.48$.

g	z_0/L	$\mathcal{N}(z_0)$	g^*	κ^*	$\Delta\kappa^*$
−0.024	1.85	3.4	−0.088	0.837	−0.075
−0.020	1.80	3.6	−0.075	0.851	−0.061
−0.016	1.80	3.8	−0.061	0.864	−0.048
−0.012	1.80	4.1	−0.047	0.879	−0.033
−0.008	1.80	4.4	−0.032	0.888	−0.024
−0.004	1.85	4.7	−0.016	0.890	−0.022
0.000	1.90	5.0	0.000	0.912	0.000
0.004	1.95	5.5	0.019	0.939	0.027
0.006	2.00	5.7	0.030	0.943	0.031
0.008	2.10	6.0	0.043	0.974	0.062
0.010	2.20	6.3	0.058	0.992	0.080
0.011	2.30	6.5	0.068	1.010	0.098
0.012	2.70	7.1	0.084	1.047	0.135

to characterize the *pure* gravity dependence of the effective thermal conductivity κ^* at a given value of ε, we define

$$\Delta\kappa^*(\varepsilon, g^*) \equiv \kappa^*(\varepsilon, g^*) - \kappa^*(\varepsilon, 0). \tag{33}$$

The values of $\Delta\kappa^*$ for the corresponding fixed values of ε_0 are also included in tables 2–5 and are plotted in figure 7. It is observed in figure 7 that, although somewhat scattered, the points tend to lie on smooth curves. The behaviour of $\Delta\kappa^*$ is in qualitative agreement with the theoretical predictions for Maxwell molecules, equations (6) and (7). More specifically, the departure from the Fourier law, as measured by $\Delta\kappa^*$, is positive when the gravity field is parallel to the heat flux ($g^* > 0$), while it is negative when both vectors are mutually antiparallel ($g^* < 0$). In addition, the magnitude of the deviation is larger in the former case than in the latter, i.e. $\Delta\kappa^*(\varepsilon, g^*) > -\Delta\kappa^*(\varepsilon, -g^*)$. From figure 7 we can also conclude that the gravity influence is less dramatic when the boundary effects are more important, since $|\Delta\kappa^*|$ tends to be smaller in the case of boundary conditions of Type I. From the data corresponding to the boundary conditions of Type II we can estimate that $\Delta\kappa^*(\varepsilon, g^*) \simeq B\varepsilon g^* + \cdots$, where the coefficient B has a value between 2 and 2.5. This is about 4 times smaller than the exact coefficient $B = 46/5$ obtained in the case of Maxwell molecules. We are not able at present to

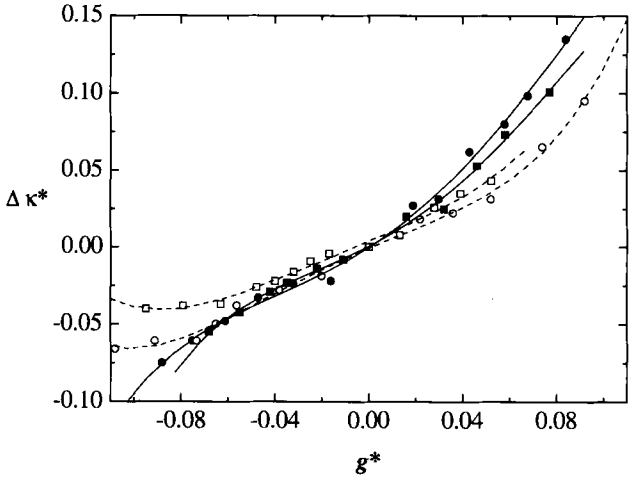

Figure 7. Plot of $\Delta\kappa^*$ versus the reduced field strength g^* for $T_- = 0.05$ with boundary conditions of Type I (□, $\varepsilon = 0.33$), $T_- = 0.05$ with boundary conditions of Type II (■, $\varepsilon = 0.36$), $T_- = 0.01$ with boundary conditions of Type I (○, $\varepsilon = 0.44$) and $T_- = 0.01$ with boundary conditions of Type II (●, $\varepsilon = 0.48$). The lines are polynomial fits to guide the eye.

elucidate which part of this discrepancy in the numerical value of B is attributable to boundary effects still present in our simulation results and which part is due to the role played by the interaction. Besides, when comparing results obtained with different interactions, one must have in mind that the choice of appropriate dimensionless parameters is not unique. In our case, we have defined ε, equation (3), and g^*, equation (4), by using the mean free path given by equation (5), which is based on the BGK model. If, on the other hand, we had used the standard mean free path of hard spheres, equation (5), then we would have $\Delta\kappa^*(\varepsilon, g^*) \simeq B'\varepsilon g^* + \cdots$, where $B' = (\lambda/\lambda')^2 B \simeq 2.76B$.

5. Conclusions

In this paper we have numerically solved the Boltzmann equation (by means of the DSMC method) for a steady heat conduction problem of hard spheres in the presence of a gravity field. The gas is enclosed between two parallel plates separated a distance equal to $L = 10$ (average) mean free paths. Two different temperature ratios ($T_-/T_+ = 0.01$ and $T_-/T_+ = 0.05$) and two alternative types of boundary conditions (boundary effects being more important in the case of Type I than in the case of Type II) have been considered. For each one of these four possibilities we have applied 12 or 13 different values of a constant gravity field $\mathbf{g} = -g\hat{\mathbf{z}}$ normal to the plates. The sign criterion is such that $g > 0$ means a field antiparallel to the thermal gradient (and hence parallel to the heat flux vector), while $g < 0$ means the opposite.

The first conclusion we draw from the results is that the hydrodynamic profiles are rather sensitive to the value of g. While the pressure p is roughly uniform if $g = 0$, it decreases (increases) with z if $g > 0$ ($g < 0$), this effect being more important as the magnitude of g grows. This is not surprising since it is an extension to non-equilibrium states of the equilibrium barometric law $p(z) \propto \exp(-mgz/k_B T)$. A less obvious effect appears in the case of the temperature profile. If there were no temperature jumps at the walls, the temperature of the gas would change from T_- at $z = 0$ to T_+ at $z = L$, irrespective of the value of g. However, due to unavoidable boundary effects, $T(0) > T_-$ and $T(L) < T_+$. Our simulation results show that the temperature jump at the cold (hot) wall decreases as the value of g increases (decreases). For instance, in the case $T_- = 0.05$ with boundary conditions of Type II, $T(0) - T_- \simeq 0.04$ and $T_+ - T(L) \simeq 0.04$ for $g = -0.016$, while $T(0) - T_- \simeq 0.01$ and $T_+ - T(L) \simeq 0.20$ for $g = 0.012$. In other words, the temperature jump at a wall decreases as the relative density near that wall increases. The more positive (negative) g is, the larger the density is near the cold (hot) wall and the smaller the temperature jump is. Since the temperature jump is more important near the hot wall, a side effect of the above discussion is that the (average) thermal gradient across the system increases when g decreases, so that it is larger for $g > 0$ than for $g < 0$. A larger thermal gradient implies a larger magnitude of the heat flux and this expectation is confirmed by our simulation results, which show that $|q_z|$ clearly increases as g decreases.

Our interest has not focused, however, on the *absolute* change of the heat flux due to the gravity field, but on its change *relative* to the Navier–Stokes prediction when the *actual* temperature gradient is considered. To that end we have introduced the ratio κ^* defined by equation (2), which is a local quantity that in the *bulk* region is expected to depend on space only through a functional dependence on the reduced thermal gradient ε, equation (3), and gravity strength g^*, equation (4). For each one of the four different combinations of T_-/T_+ and boundary conditions we have fixed a value $\varepsilon = \varepsilon_0$ ($\varepsilon_0 \simeq 0.3$–0.5) and have analysed the g^* dependence of $\Delta\kappa^*(\varepsilon_0, g^*) \equiv \kappa^*(\varepsilon_0, g^*) - \kappa^*(\varepsilon_0, 0)$. The simulation results for hard spheres presented in this paper are in qualitative agreement with those obtained for Maxwell molecules by a perturbation analysis of the Boltzmann [15] and the BGK [16] equations. More specifically, when the field and the heat flux are parallel ($g^* > 0$) the gravity induces an enhancement of the (relative) heat conduction ($\Delta\kappa^* > 0$), while the opposite happens when both vectors are mutually antiparallel. In addition, the influence of gravity is more pronounced in the former case than in the latter. At a quantitative

level, on the other hand, the values of $|\Delta\kappa^*|$ reported here are typically smaller than those theoretically estimated for comparable values of ε and g^*. A certain part of this difference is possibly due to boundary effects still present in our simulations and absent in the theoretical analyses of [15, 16]. This expectation is supported by the fact that $|\Delta\kappa^*|$ is generally smaller in the case of conditions of Type I than in that of Type II, thus indicating that boundary effects tend to mitigate the influence of gravity. Notwithstanding this, the remaining difference leads us to conclude that the response of the system to the application of the field, as measured by $\Delta\kappa^*$, is less important in the case of hard spheres than in the case of Maxwell molecules.

The authors are grateful to J. M. Montanero for his help in the simulation method. This work has been done under the auspices of the Agencia Española de Cooperación Internacional (Programa de Cooperación Interuniversitaria Hispano-Marroquí). A.S. acknowledges partial support from the DGES (Spain) through Grant No. PB97-1501 and from the Junta de Extremadura (Fondo Social Europeo) through Grant No. IPR98C019.

References

[1] Ciccotti, G., and Tenenbaum, A., 1980, *J. statist. Phys.*, **23,** 767; Tenenbaum, A., Ciccotti, G., and Gallico, R., 1982, *Phys. Rev.* A, **225,** 2778.

[2] Mareschal, M., Kestemont, E., Baras, F., Clementi, E., and Nicolis, G., 1987, *Phys. Rev.* A, **35,** 3883; Clause, P.-J., and Mareschal, M., 1988, *Phys. Rev.* A, **38,** 4241.

[3] Montanero, J. M., Alaoui, M., Santos, A., and Garzó, V., 1994, *Phys. Rev.* E, **49,** 367.

[4] Asmolov, E. S., Makashev, N. K., and Nosik, V. I., 1979, *Dokl. Akad. Nauk SSSR*, **249,** 577 [*Sov. Phys. Dokl.*, **24,** 892].

[5] Santos, A., Brey, J. J., and Garzó, V., 1986, *Phys. Rev.* A, **34,** 5047.

[6] Santos, A., Brey, J. J., Kim, C. S., and Dufty, J. W., 1989, *Phys. Rev.* A, **39,** 320.

[7] Kim, C. S., Dufty, J. W., Santos, A., and Brey, J. J., 1989, *Phys. Rev.* A, **39,** 328.

[8] Kim, C. S., and Dufty, J. W., 1989, *Phys. Rev.* A, **40,** 6723.

[9] See Maxwell, J. C., 1867, *Phil. Trans. Roy. Soc.* (London), **157,** 49; reprinted in Brush, S. G., 1966, *Kinetic Theory, Vol. 2, Irreversible Processes* (Oxford: Pergamon). In this paper, Maxwell analysed the encounters of molecules repelling each other with forces inversely proportional to the nth power of the distance and found that the variation of mean values of functions of the velocity due to encounters included the power $V^{(n-5)/(n-1)}$ of the relative velocity V of the two colliding molecules. In the case of inverse fifth-power forces ($n = 5$), the relative velocity drops out and the integrations can be carried out without knowing the non-equilibrium distribution function. These fictitious particles interacting with a repulsive force inversely proportional to the fifth power of their distance are called Maxwell molecules.

[10] Bhatnagar, P. L., Gross, E. P., and Krook, M., 1954, *Phys. Rev.* A, **94,** 511; Welander, P., 1954, *Ark. Fys.*, **7,** 507.

[11] Iribarne, J. V., and Cho, H.-R., 1980, *Atmospheric Physics* (Dordrecht: Kluwer), Ch. 1.

[12] Chamberlain, J. W., 1978, *Theory of Planetary Atmospheres. An Introduction to Their Physics and Chemistry* (New York: Academic Press), App. III.

[13] Chapman, S., Cowling, T. G., 1970, *The Mathematical Theory of Non-Uniform Gases* (Cambridge: Cambridge University Press).

[14] Cercignani, C., 1990, *Mathematical Methods in Kinetic Theory* (New York: Plenum).

[15] Tij, M., Garzó, V., and Santos, A., 1997, *Phys. Rev.* E, **56,** 6729.

[16] Tij, M., Garzó, V., and Santos, A., 1999, *Rarefied Gas Dynamics* Vol. 1, edited by R. Brun, R. Campargue, R. Gatignol and J.-C. Lengrand (Toulouse: Cépaduès), pp. 239–246.

[17] Doi, T., Santos, A., and Tij, M., 1999, *Phys. Fluids*, **11,** 3553.

[18] Tij, M., Garzó, V., and Santos, A., 1999, *Phys. Fluids*, **11,** 893.

[19] Hansen, J.-P., and McDonald, I. R., 1986, *Theory of Simple Liquids* (London: Academic Press).

[20] Bird, G., 1994, *Molecular Gas Dynamics and the Direct Simulation of Gas Flows* (Oxford: Clarendon Press).

[21] Dorfman, J. R., and van Beijeren, H., 1977, *Statistical Mechanics*, Part B, edited by B. J. Berne (New York: Plenum), pp. 65–179.

[22] Wadsworth, D. C., 1993, *Phys. Fluids* A, **5,** 1831.

[23] Alexander, F. J., and Garcia, A. L., 1997, *Comput. Phys.*, **11,** 588.

[24] Cercignani, C., and Cortese, S., 1994, *J. statist. Phys.*, **75,** 817; Montanero, J. M., Santos, A. and Garzó, V., 1996, *Phys. Fluids*, **8,** 1981.